



RESEARCH ARTICLE

10.1029/2020JD033881

Tracking the Stratosphere-to-Surface Impact of Sudden Stratospheric Warmings

Key Points:

- We develop a tracking algorithm to estimate the date of surface impact of sudden stratospheric warmings (SSWs)
- The method enables separation of the timings and magnitudes of surface impacts of displacement and split SSWs
- The method will be a valuable tool for use with climate models

Richard J. Hall¹ , Daniel M. Mitchell¹ , William J. M. Seviour² , and Corwin J. Wright³ 

¹School of Geographical Sciences, Cabot Institute for the Environment, University of Bristol, Bristol, UK, ²Global Systems Institute and Department of Mathematics, University of Exeter, Exeter, UK, ³Centre for Space, Atmospheric and Oceanic Science, University of Bath, Bath, UK

Supporting Information:

- Figure S1

Correspondence to:

R. J. Hall,
richard.j.hall@bristol.ac.uk

Citation:

Hall, R. J., Mitchell, D. M., Seviour, W. J. M., & Wright, C. J. (2021). Tracking the stratosphere-to-surface impact of Sudden Stratospheric Warmings. *Journal of Geophysical Research: Atmospheres*, 126, e2020JD033881. <https://doi.org/10.1029/2020JD033881>

Received 11 SEP 2020
 Accepted 21 DEC 2020

Abstract Sudden stratospheric warming (SSW) events are extreme atmospheric regimes which can have a signature in surface weather up to 40 days after event onset in the stratosphere. SSWs can be classified as either vortex splitting or vortex displacement events, with the nature and timing of the surface impact potentially being different between the two. In this study, using ERA40/Interim reanalysis data, we develop a simple empirical downward tracking algorithm which for the first time allows us to estimate the time of surface impact for individual SSW events. We show that the surface impact following splitting events is, on average, about 1 week earlier than following displacement events, albeit with considerable variability. By compositing tropospheric responses around the identified date of surface impact, rather than around the central stratospheric onset date as common in previous studies, we can better constrain the surface signal of SSWs. We find that while the difference in North Atlantic Oscillation anomalies between split and displacement vortices is small, surface temperature anomalies over northwest Europe and northern Eurasia are significantly colder for splitting events, particularly over the UK just prior to the surface impact date. Displacement events on average are wetter over Northwest Europe around the time of surface impact, consistent with the jet stream being displaced further south in response to split events. Our downtracking algorithm can be used with any reanalyses and gridded model data, and therefore will be a valuable tool for use with the latest climate models.

1. Introduction

In winter, a polar vortex develops in the stratosphere (the stratospheric polar vortex; SPV), with strong westerly zonal winds blowing around a region of low temperatures roughly located over the pole. On occasion, most often in the Northern Hemisphere, the SPV can break down, in what is known as a sudden stratospheric warming (SSW), one of the most dramatic of atmospheric phenomena (M. P. Baldwin et al., 2021). First described by Scherhag (1952) they involve the rapid warming of the SPV with temperatures increasing by up to 30–40 K over 1–2 days (Butler et al., 2017). The zonal mean westerly winds at 10 hPa and 60°N reverse, and this is typically used as the definition of an SSW (for more details see Butler et al., 2017). SSWs occur on average around 6 times a decade, although the observational record is short and there is considerable interdecadal variability in occurrence (Charlton & Polvani, 2007; hereafter CP07). While some uncertainty remains as to the driving mechanisms of SSWs, most are believed to be related to internal resonances of the SPV (e.g., N. J. Matthewman & Esler, 2011) and to the vertical propagation of planetary waves from the troposphere, often associated with tropospheric blocking (Martius et al., 2009), which then break and interact with the mean flow (Matsuno, 1971; Polvani & Waugh, 2004).

SSWs are important as they can impact upon mid-latitude weather, typically over a period up to 40 days after an SSW (M. P. Baldwin & Dunkerton, 2001). The weakening of the vortex can favor an equatorward shift of the tropospheric jet and storm tracks over the Atlantic (Kidston et al., 2015). Focusing on SSW impacts on European weather, cold air outbreaks can occur over Eurasia and northwestern (NW) Europe (Kolstad et al 2010; Lehtonen & Karpechko, 2016; Mitchell et al., 2013; Tomassini et al., 2012). For example, the “Beast from the East” cold air outbreak over NW Europe at the start of March 2018 was associated with a SSW onset in mid-February (e.g., Karpechko et al., 2018; Overland et al., 2020). Kolstad et al. (2010) found that the probability of cold air outbreaks increased by 50% or more in some parts of Europe during an SSW, as a consequence of changing pressure patterns leading to altered temperature advection. Tomassini et al. (2012) showed that the weaker SPV leads to a lowering of the tropopause at high latitudes, with a

© 2020 The Authors.

This is an open access article under the terms of the [Creative Commons Attribution License](https://creativecommons.org/licenses/by/4.0/), which permits use, distribution and reproduction in any medium, provided the original work is properly cited.

tendency to higher pressure below, resulting in the advection of cold air toward northern Europe from the Arctic. More recently however, Lehtonen and Karpechko (2016) argued that SSWs provide only limited predictability of cold air outbreaks as many of these are coupled to atmospheric blocking events which can be precursors to the SSW events (Martius, 2009). King et al. (2019) also identified cooler than average European temperatures prior to SSW onset but found that the intensity of cold extremes was greatest after the event. SSW events have an impact on the North Atlantic Oscillation (NAO), but uncertainty remains as to the impacts on other North Atlantic weather regimes such as the European and Scandinavian blocking patterns (Beerli & Grams, 2019; Charlton-Perez et al., 2018). These impacts on surface weather mean that SSWs can have significant socio-economic consequences and their identification can enhance subseasonal weather forecasting skill (e.g., Domeisen et al., 2020a).

SSWs are commonly classified as either split or displacement events, depending on whether the vortex is displaced from over the pole, or whether it is split into two distinct vortices. CP07 base this distinction on absolute vorticity, while Mitchell et al. (2011, 2013) and W. J. M. Seviour et al. (2013) use vortex moment diagnostics of the potential vorticity or geopotential height fields to classify the event. There is considerable debate concerning any differences between the impacts of split and displaced vortices. Split events are more barotropic in the stratosphere (e.g., N. J. Matthewman & Esler, 2011). Mitchell et al. (2013) and W. J. M. Seviour et al. (2013, 2016) identify a stronger surface signal at shorter time lags for split as opposed to displacement events, with positive (negative) temperature anomalies over North America (Eurasia) (Mitchell et al., 2013). Others (CP07; Cohen & Jones, 2011) find little difference in surface characteristics, based on reanalysis data. However, a fundamental aspect of this comparison is that such studies are not comparing like with like; for example, the former define SSWs using a zonally asymmetric moment diagnostics approach (Waugh, 1997) while the latter are based on zonal-mean wind reversal. The different approaches can identify different SSW onset dates, as well as classifying events differently; only around half of the onset dates of Mitchell et al. (2013) and CP07 are consistent. These two approaches generate different sets of events, with different surface impacts. Furthermore, any differences seen in surface impact in these studies are for multievent means, often averaged over quite long time periods relative to SSW onset at 10 hPa, ranging from 30 days (e.g., Mitchell et al., 2013) up to 60 days (CP07), which means the probability distribution of the timings of surface impacts is unknown and differences between event types are smoothed out, as the time taken for an event to impact the surface varies considerably.

In addition, the studies above do not distinguish between SSWs that couple with the troposphere and those whose impacts are limited to the stratosphere. In the zonal mean, nearly half of SSWs identified in reanalyses show no significant, long-lasting impacts on the Northern Annular Mode (NAM, Karpechko et al., 2017). However, a key region for SSW impact is the Atlantic sector. By using the NAO to determine whether SSWs produce a surface signature, Domeisen (2019) found that a greater number (around two-thirds) of SSW events had a surface signature in the North Atlantic region, manifesting as a shift to a negative NAO following the SSW, with a southward displacement of the jet stream.

In this study we develop a novel SSW tracking algorithm that addresses some of the issues discussed above. The tracking algorithm is an empirical approach based on physical characteristics of the atmosphere and enables an estimation of the date of surface impact for each SSW event. This in turn gives an estimation of a probability distribution of the lag between SSW onset near the stratopause and the surface impact, which we anticipate may be of value for medium-range forecasting. Our approach also aims to enable a new comparison of the impacts of split and displacement events, by aligning the comparison on the date of impact rather than onset date and avoiding the loss of signal resulting from averaging over a broad window relative to SSW onset at 10 hPa.

2. Data

For our analysis ERA-Interim data (ERA-I, Dee et al., 2011) are used and daily means are calculated from the 4x daily data for 1979–2019. To increase the sample size, we extend the data back to 1957 using ERA 40 (Uppala et al., 2005). While ERA 40 includes presatellite era data, it has been shown to be suitable for identifying SSW onset dates and classification, and for assessing downward coupling to the troposphere (Gerber et al., 2021). Twenty-three common vertical levels are used from the two reanalyses.

Table 1
List of Sudden Stratospheric Warmings (SSWs), Their Classification, Downward or No Downward Response (dSSW/nSSW) and the Lag From Start of Tracking at 1 hPa to Surface, Using Both 23 and 8 Levels

SSW date	Split/ displaced	dSSW/ nSSW	Lag 23 level	Lag 8 level
January 31, 1958	S	dSSW	34	33
January 17, 1960	D	dSSW	0	8
January 28, 1963	S	dSSW	25 ^a	20 ^a
December 16, 1965	D	dSSW	5 ^a	28
February 23, 1966	S	nSSW	14	1
January 7, 1968	S	dSSW	9	5
November 28, 1968	D	dSSW	24	30
March 13, 1969	D	nSSW	7	7
January 2, 1970	D	nSSW	10	8
January 18, 1971	S	nSSW	22	22
March 20, 1971	S	dSSW	7	8
January 31, 1973	S	nSSW	24	23
January 9, 1977	S	dSSW	9	3
February 22, 1979	S	dSSW	18	17
February 29, 1980	D	dSSW	25	24
March 4, 1981	D	dSSW	2	2
December 4, 1981	D	dSSW	6	4
February 24, 1984	D	dSSW	28	19
January 1, 1985	S	dSSW	18	17
January 23, 1987	D	nSSW	45 ^a	43 ^a
December 8, 1987	S	nSSW	3	0
March 14, 1988	S	dSSW	7	5
February 21, 1989	S	nSSW	31	20
December 15, 1998	D	dSSW	22	22
February 26, 1999	S	dSSW	9	2
March 20, 2000	D	dSSW	26	25
February 11, 2001	D	dSSW	19	6
December 30, 2001	D	nSSW	7	3
January 18, 2003	S	nSSW	5	4
January 5, 2004	D	dSSW	34	36
January 21, 2006	D	dSSW	24 ^a	22 ^a
February 24, 2007	D	nSSW	11	11
February 22, 2008	D	dSSW	34	32
January 24, 2009	S	dSSW	22	15
February 9, 2010	S	dSSW	24	4
March 24, 2010	D	dSSW	7	17
January 6, 2013	S	dSSW	12	7
February 12, 2018	S	dSSW	15	10
January 2, 2019	S	nSSW	37	35

^aDenotes algorithm-sensitive events.

The polar cap height anomaly (PCH) at each vertical level is used to track the downward progression of the SSWs. Geopotential height anomalies at each level are calculated as the mean for each day of the year over all years, divided by the standard deviation for the relevant day. These anomalies are averaged over the region 65°N–90°N for each level to give PCH anomalies. 65°N–90°N is used as averaging over this range gives the highest correlation with the NAM index (M. P. Baldwin & Thompson, 2009).

To further examine surface responses, we use daily mean 2 m air temperature (hereafter referred to as surface temperature) and total daily accumulated precipitation, averaged over NW Europe (10°W–20°E, 48°N–65°N). This region was selected to have a consistent sign of correlation with the NAO, corresponding to one center of a quadrupole of temperature anomalies around the Atlantic basin associated with the NAO (e.g., Clark & Feldstein, 2020). For these data sets, we use daily anomalies from the climatological seasonal cycle (i.e., the average daily value over all years) to give a better indication of the magnitude of the anomalies. To place the NW European anomalies in a wider context, we assess surface temperature and precipitation anomaly data from –20°E to 40°E, 25°N–75°N, and the whole of the Northern Hemisphere. In addition, standardized anomalies of surface temperature are used for comparison with the magnitude of NAO and Arctic Oscillation (AO) responses to SSW events.

The latitude of the North Atlantic eddy-driven jet is calculated according to Woollings et al. (2010). The zonal mean 850 hPa zonal wind over –60°W to 0°W, 15°N to 75°N is calculated for each degree of latitude, with the wind field filtered using a low-pass 61-point Lanczos filter (Duchon, 1979) to remove synoptic-scale variability. The jet latitude for each day is simply the latitude at which the maximum zonal mean zonal wind occurs.

To identify which SSW events precede significant tropospheric anomalies in the North Atlantic sector, and to identify SSW influences on large-scale circulation indices, we use a daily NAO index provided by NOAA Climate Prediction Center (CPC) (<https://psl.noaa.gov>). This index identifies the NAO using rotated empirical orthogonal function (EOF) analysis of 500 hPa height anomalies. To compare with a zonally averaged surface impact, we use the AO/NAM index, also from CPC, which is the leading EOF of monthly mean 1,000 hPa geopotential height anomalies, 20°N–90°N. For direct comparison purposes we restandardize the two indices so that they have the same variance, but otherwise we use the indices as provided.

3. Methods

3.1. SSW Onset Identification

We use the method of identifying SSW onset described in CP07, based on reversal of zonal mean winds at 10 hPa and 60°N, for the months November to April. We require at least 20 consecutive days of westerly winds at this latitude and pressure level between each defined SSW event. Final warmings are eliminated by ensuring that the mean zonal winds return to westerlies for at least 10 consecutive days prior to April 30th of the relevant year. A list of dates of SSW onset provided in CP07 and updated by Butler et al., 2017 is shown in Table 1.

3.2. SSW Classification

The SSWs are classified into split and displaced vortex events according to the absolute-vorticity-based classification method presented by CP07. SSWs after 2007 are classified on the basis of a number of subsequent papers using the CP07 approach (e.g., Gerber et al., 2021; Lee & Butler, 2020). Classification of SSWs is by no means clear cut. Around a third of observed SSWs cannot be classified unambiguously as split or displaced events (Gerber et al., 2021), with many events exhibiting aspects of both splits and displacement. Different detection methods also contribute to the lack of clarity. In addition to the CP07 method, we also adopt a variant method, where the central dates of the SSW are defined according to the wind reversal method (CP07), but splits and displacements are classified by application of the vortex moment diagnostics method of W. J. M. Seviour et al. (2013) to the 10 days either side of the onset date. The event is classified as split or displacement depending on whether the aspect ratio or centroid latitude diagnosis threshold is exceeded more often during the 20-day window (Gerber et al., 2021) and results are presented as supplementary information. A further method proposed by Lehtonen and Karpechko (2016) is not used here, as only a single event is classified differently from the CP07 method.

3.3. Downward Impact of SSWs

As our primary focus is on the Atlantic sector, where the largest surface impacts of SSWs have been identified, to identify which SSWs have a surface expression we adapt the method developed by Domeisen (2019), hereafter D19. This uses the NAO index and identifies SSWs with a surface signature as those events that are either followed by a persistent negative NAO or a subsequent switch from a positive to negative NAO. D19 used a station-based NAO (Cropper et al., 2015). However, here we use an EOF-derived NAO, which has reduced variance and extends beyond 2014 to include the most recent SSWs. As a consequence of the reduced variance we adjust the original metrics to produce a similar proportion of surface impacting/nonimpacting SSWs. A persistence event is identified if for a 45-day window from 8 to 52 days after the SSW central date (as in D19), the mean daily NAO is negative, and the proportion of negative NAO days within this period exceeds 0.45, adjusted from 0.5 in D19, so as to match the D19 classification. A switch NAO is identified where there is a drop greater than 0.5σ between two 11-day periods. Again, this is reduced from the D19 value of 1σ to reflect the reduced variance of the EOF time series. As in D19, the mean NAO over the initial period, (i.e., the 11 days up to and including the SSW central date) is required to be positive, while the mean over the second 11 days must be negative. The mean for the second period is calculated using an 11-day moving window from 1 to 19 days after the event and needs to be negative only in one of the overlapping moving windows.

3.4. Downward Tracking of SSWs

We develop an algorithm to produce a plausible downward track of the SSW through time, to allow an estimate of the time of surface impact for each event. While the method is empirical, and therefore cannot explicitly demonstrate causality, it is objective and based on physical characteristics of the atmosphere, and we propose that it can provide valuable new insights into the timing of the surface impacts of SSWs.

The temporal location of the downward progression is defined as the maximum PCH anomaly within a time window at a given level, subject to a number of factors explained below. The location of the window is determined by the identified day of the downward tracking at the level above. The downward tracking starts at 1 hPa, identified as the maximum PCH anomaly in a window extending 10 days either side of the 10 hPa onset in Butler et al. (2017), allowing for the difference in level and that PCH is a different variable to that used in the identification method (zonal mean wind reversal).

The maximum rate of downward progression is constrained to be physically plausible by the dynamical timescales identified for the NAM at different levels, defined by Charlton-Perez and O'Neill (2009) (CON09). In CON09 the daily annular mode index is high-pass filtered, as low frequency oscillations in the annular mode can unduly influence the autocorrelation structure. Figure 7a of CON09 shows dynamical timescales identified for an atmosphere with a realistic radiative time-scale profile and orographic forcing. The following algorithm is applied to identify the window size for each subsequent level.

1. Based on CON09, the atmosphere is divided into three layers: 1–30 hPa, 30–200 hPa, and 200–1,000 hPa. Dynamical timescales for each, averaged from CON09 are shown in Table 2, together with total vertical distance Σdz for the levels. Dividing Σdz by the dynamical timescale gives what can be regarded as a maximum vertical descent rate in meters per day
2. The rate of downward progression between levels is determined by the vertical distance dz between each level and the vertical descent rate, which are combined to give a window width in which the SSW propagation can occur at each subsequent level (Table 3). The start index of the window is set at the index of the maximum value selected at the level above. The end index of the window is determined by 5 ($dz/\text{descent rate}$). The scaling factor (5) is required as dividing dz by the descent rate produces unrealistically short windows
3. Below 700 hPa, the track is set to move downwards vertically as any shift in time at these levels is unrealistic since downward progression tends to be barotropic in the troposphere

Thirty-nine SSW events are identified using the CP07 method. Thirty-five of these had a clear continuous track of positive PCH anomalies (negative NAM), while four events were more sensitive to the algorithm and are indicated in Table 1. Using a modified algorithm as outlined in the supplementary material (Text S1) based on identifying relative maxima within the time window, of the 27 downward propagating SSWs identified in Table 1, 10 SSWs had identical lags and a further 10 were within ± 4 days of the surface date identified here. Where differences were greater than four days between the algorithm variants, it is often plausible alternative SSW tracks that are identified. Figure 1 presents four examples of SSW downtracking: displacement (Figure 1a) and split (Figure 1b) events, together with two events that are particularly algorithm-sensitive (Figures 1c and 1d). In one, the track is overconstrained by the large PCH anomaly extending downwards to around 100 hPa (Figure 1c), while for the other, the track looks plausible, but below 100 hPa follows a set of anomalies that dissipate above the surface, leaving the track in a dead end (Figure 1d). Tracks for these two events using a variant of the algorithm are shown in Figure S1.

To assess sensitivity, the tracks were recalculated for ERA-I data only, using climatological standardized anomalies for the period 1979–2019, for the full 37 levels available and for the 23 levels common to ERA40. Twenty-six events were assessed, of which four were sensitive to the change in number of levels, with a difference in descent time greater than 6 days. Perhaps more importantly, 23 (21) of the events in the 23-level (37-level) ERA-I -only data sets had surface impact dates differing by no more than 2 days from those of the combined data set.

3.5. Using the Algorithm With Reduced Levels (e.g., The CMIP6 Repository)

The number of atmospheric levels stored varies between data sets, and especially between reanalyses and free-running models. In ERA-I daily data are available on 37 vertical levels, ERA40 has 23 available levels, while in the CMIP6 archive, eight levels are the standard for daily data storage, even though the individual models may have had many more vertical levels in their original configurations. Large-scale multimodel comparison projects such as CMIP6 in general do not prioritize data output for many stratospheric levels. The tracking algorithm was applied to the ERA data using the CMIP6 levels only, to ensure that the method is robust to reduced stratospheric level density. This enables future applications to model output data.

Initially, many lags were far too long with unrealistic jumps between levels, particularly in the stratosphere, due to missing levels. When using 23 levels, the windows of successive levels always overlap to some extent. For example, between 10 and 50 hPa, there are an additional two levels in ERA-I/ERA40, meaning four levels span this gap, with overlapping windows. However, if the algorithm is used unmodified for eight levels, these windows are effectively placed end to end. This results in unrealistically large windows and the facility to make similarly unlikely jumps in time. Furthermore, the cutoff between upper and lower stratosphere in the algorithm occurs at 30 hPa, a level that does not exist in CMIP6 and the level separating the lower stratosphere from the troposphere was set at 200 hPa, which is not available in CMIP6.

The algorithm can be tuned for use with a CMIP6-style data set by setting the level thresholds to 50 and 250 hPa respectively, and by using different scaled values for descent. This results in plausible track identifications for 36 out of 39 SSWs. Window sizes for CMIP6 are shown in Table 3.

Table 2
Summary of Distance Between Levels, Dynamical Timescales, and Descent Rates Used in the Downtracking Algorithm

Levels (hPa)	Σdz (m)	Dynamical timescale (days)	Descent rate (D) $\Sigma dz /$ timescale (m day ⁻¹)	Scaled Value D/5
1– <30	23,808	22	1,082.2	216
30– <200	13,280	16	830	166
≥200	11,266	10	1,126.6	225

There is a good correspondence between lags identified for most of the 39 SSW events using different numbers of vertical levels (Figure 2). Eighteen levels are used for the ERA-I/40 downtracking, removing the track above 10 hPa, to allow for a better comparison of tracking over the same vertical distance. The correlation between lags for 8 and 18 levels is higher for split than displaced events (0.97 cf. 0.84). Four displacement events have an appreciably longer lag over eight levels. For the 8-level cases, the large jumps in time occur at lower stratospheric or tropospheric levels (100–250 hPa, 250–500 hPa), suggesting that the window sizes here are large relative to those used for the main algorithm, however the tracks produced reach the surface at plausible points, even though vertical movement is less tightly constrained.

We must emphasize that the algorithm does not necessarily indicate a physical mechanism but is purely a method for linking the descent of anomalies and estimating the time of surface impact. Such an approach will necessarily involve some subjective parameter choices as outlined above.

Table 3
Pressure Levels, dz, and Window Size at Each Level for Combined ERA-I/40 Data Over 23 Levels, and for ERA-I/40 Data Selected for the 8 CMIP6 Levels Only

Pressure level (hPa) ERA-I/40	dz/m	Window size	Pressure level (hPa) CMIP6	dz/m	Window size
1		20			
2	4,852	23			
3	2,838	14			
5	3,576	18			
7	2,355	12			
10	2,497	13	10		20
20	4,852	23			
30	2,838	14			
50	3,576	23	50	11,266	34
70	2,355	15			
100	2,497	16	100	4,852	15
150	2,838	18			
200	2,014	13			
250	1,562	8	250	6,414	19
300	1,276	7			
400	2,014	10			
500	1,562	8	500	4,852	11
600	1,276	7			
700	1,079	6	700	2,355	6
775	712	1			
850	647	1	850	1,359	1
925	592	1			
1,000	546	1	1,000	1,138	1

Note. The starting window in each case is preset at 20.

3.6. Statistics

The significance of differences between median lags for split and displacement SSWs is assessed using the two-sided nonparametric Mann-Whitney U test. For spatial plots, the statistical significance of the difference between means of splits and displacements is assessed using a permutation test with pooling of splits and displacements and 10,000 random reshufflings of the data, before separating the events into two groups equal to the number of splits and displacements. Means are calculated for each group and the significance of their difference is stored. The observed mean values are then compared with this distribution to assess significance. A one sample t-test is used to assess whether the mean value for splits or displacements is significantly different from climatological values. With such small sample sizes significance should be treated with caution and is here used as a guide to indicate where associations with surface weather are strongest. Significance is reported at the 5% and 10% levels.

4. Results

4.1. Downward Progression

Most events with a tropospheric signal are consistent with those identified by D19. However, there is some variation among more marginal events. D19 identified 27 downward-progressing events excluding 2018, while here 27 are identified inclusive of the 2018 SSW (Table 1). Any differences in event selection arise due to adjusted thresholds and the use of a different EOF-based NAO time series. Including all identified SSW events in analysis will be a contributory factor in obscuring any differences in surface impact in the North Atlantic region as some events do not have a surface impact in the region. Using this subsetting approach allows a better exploration of the differences.

4.2. Differences in Classification of Split and Displacement Events

Applying the modified classification (Gerber et al., 2021; W. J. M. Seviour et al., 2013) to the wind reversal onset dates changes the classification of

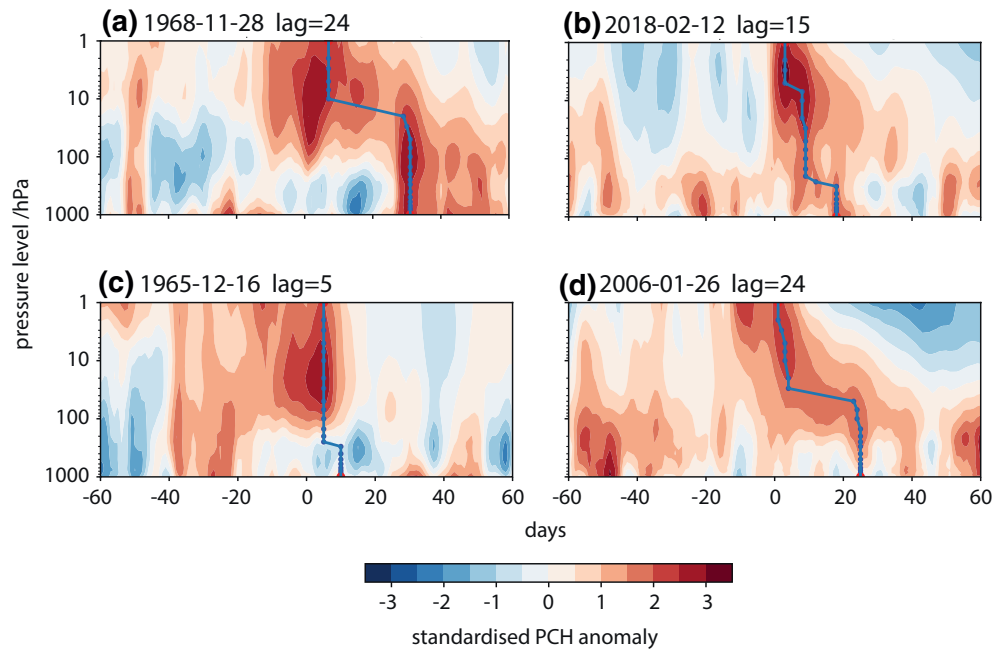


Figure 1. Examples of SSWs and downward tracking (blue dots and lines). Red dots denote start and end of tracking, plotted on polar cap height anomaly (PCH) anomalies. Plots are centered on the date of sudden stratospheric warming (SSW) onset defined in CP07 (d0). (a) A displacement event (b) a split event (c and d) are algorithm-sensitive displacement events discussed in the text.

some SSWs. Of the 27 downward-progressing events identified, six of these change classification. Specifically, four events switch from split to displacement events, one changes from displacement to split and December 4, 1981 becomes unclassifiable as it contains an irresolvable mix of split and displacement features, according to this classification. As over 20% of SSWs changed classification, aspects of the analysis were undertaken for this new classification; results are presented in SI and relevant observations are referred to below.

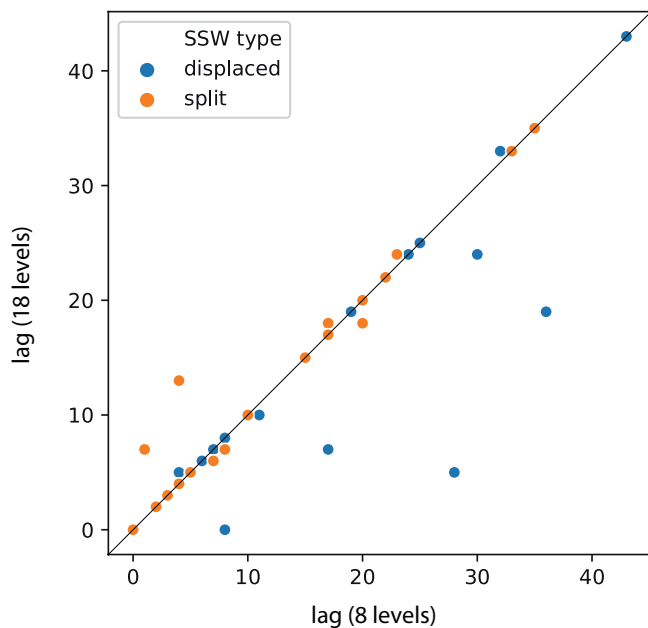


Figure 2. Scatterplot showing lags of SSW events calculated for 8 and 18 vertical levels. Correlations: displaced, $r = 0.84$; split, $r = 0.97$, overall $r = 0.89$.

4.3. Differences Between Split and Displacement SSWs

Figure 3 shows the downward tracks of all displacement (14 events) and split (13 events) SSWs that are identified as having a surface expression (Table 1). Note that the time taken to reach the surface is calculated from 1 hPa rather than the SSW onset date at 10 hPa, as downward tracking starts at 1 hPa. While there is a considerable overlap in the time taken for events to reach the surface, for displacement events we see a primary cluster of eight events with a propagation time greater than 20 days, whereas for split SSWs, only four events have a lag exceeding 20 days. The median time taken for split events is shorter than for displacement events (15 days for splits, 23 days for displacements), in agreement with other studies that identify split vortex events as more barotropic (e.g., N. J. Matthewman et al., 2009; W. J. M. Seviour et al., 2016). However, given the small sample size, this difference is not significant ($p = 0.42$) although it is notable that the median lag for displacement events lies outside the interquartile range of the split events (Figure 3c). The inclusion of the algorithm-sensitive SSW events makes little difference to the median track lags, and no difference in the case of displacements as one event lies on each side of the median. If the modified event classification is used (Gerber et al., 2021), the difference between split and displacement

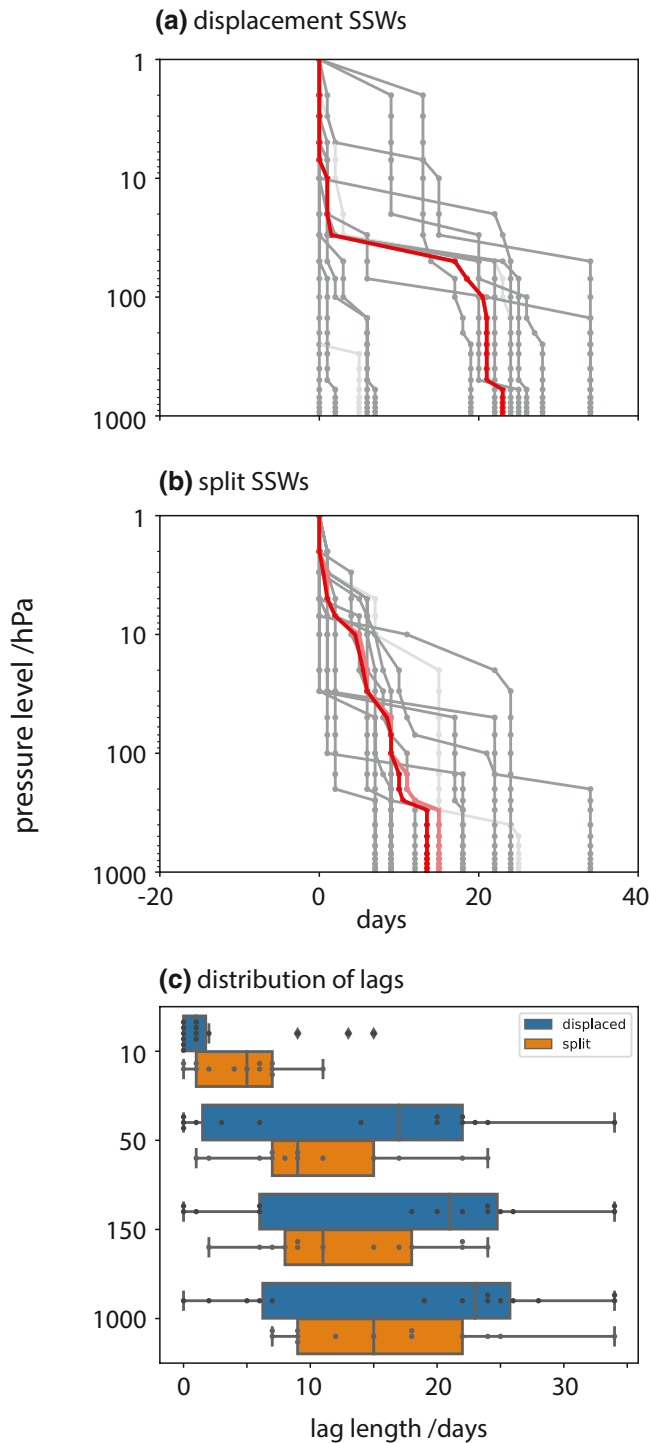


Figure 3. Downward tracks of (a) displaced SSWs and (b) split SSWs calculated by the tracking algorithm (gray). Light gray shows the tracks of the events that are particularly sensitive to the algorithm. Red shows the median at each level of the downward tracks, salmon is the median downward track including the sensitive events. In (a) there is no change in median values with the inclusion of sensitive events. (c) Distributions of lag times at different levels, divided according to SSW type (14 displacements, 13 splits). Dots indicate the location of individual events; outliers are indicated by diamonds.

lags is more pronounced, with the split and displacement median lags becoming 13.5 and 24 days respectively (Figure S2) but still not significant ($p = 0.22$).

An interesting feature of the displacement lags is that the events appear to fall into two distinct groups, that is, those with a lag of less than 10 days, and those with a lag exceeding 15 days. This arises irrespective of the classification used, or whether or not we include all 39 events in our assessment (Figures 3a and 3c; S2a, S2c, and S3). Given the small sample size, this could well be a product of sampling uncertainty. However, we note that at the time of event onset, half the short-lag displacement events are accompanied by a neutral El-Niño, and half a positive El-Niño, whereas more than half of the long-lag events are associated with La Niña events. Considering all 39 SSWs, half of all events associated with a neutral El Niño are short-lag displacement events. In addition, at onset there are more zonal and European blocking weather regimes for the long-lag events (eight out of nine events) whereas the short-lag events are more frequently accompanied by Greenland blocking (Domeisen et al, 2020b). While the sample size is small, it is possible that differences in lag time for displacement events are at least partially determined by tropospheric weather regimes at onset and may in particular be influenced by El-Niño phase. It is possible that impacts at near-zero lag may in fact be associated with precursor signals such as Ural Blocking, rather than an SSW impact.

The lag-distribution for each type of vortex event is visualized in Figures 3c, S2c, and S3. At 50 hPa and below, the median lag for split events is markedly less than that for displacement events and this figure presents evidence of the time-distribution of surface impacts of SSWs that is, not tied to SSW onset date. Considering all 39 SSW events, the difference between medians at the surface is less distinct (17 days, splits; 19 days, displacements) (Figure S3).

4.4. Surface Impacts

The identification of lag times for SSW events allows a surface impact date to be calculated for each event. Comparing events according to this date, rather than SSW onset as in most previous studies, enables a more targeted focus on the separation of the magnitude and timing of any surface impacts, potentially allowing an easier isolation of the signal from the noise.

At the identified day of surface impact there is a clear shift toward negative NAO, AO, and surface temperature anomalies for both types of SSW (Figure 4). This is in part by design through the use of the NAO as an indicator of tropospheric influence in the Atlantic region over the period following SSW onset at 10 hPa. While there is little difference between the strength of the NAO and AO for splits and displacements, the differences in temperature anomalies are greater, although not quite significant ($p = 0.14$). Patterns are very similar for the modified classification (Figure S4a). However, if all 39 events, including nondownward propagating ones are assessed, interquartile ranges for the NAO (both splits and displacements) and AO (displacement events only) extend into positive values and the temperature anomaly difference between splits and displacements is small (Figure S4b).

Using the SSWs of 2004 and 2013 as examples, there is a close correspondence between surface anomalies and the surface impact date of

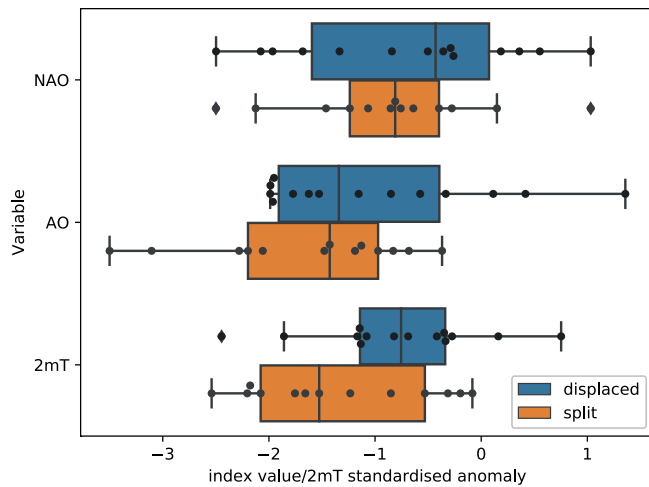


Figure 4. Rescaled North Atlantic Oscillation (NAO), Arctic Oscillation, and surface temperature standardized anomaly values for the day of each event when the SSW downward tracking reaches 1,000 hPa. Temperature anomalies calculated over region shown by red box in Figure 9.

the downtracking algorithm (Figure 5). For both types of event a clear negative surface temperature anomaly spans the surface impact date (d_0), with negative NAO values being particularly clear for the 2004 SSW around the date of surface impact (Figure 5b) and a short-lived and weakly negative NAO for 2013 (Figure 5a). In both the instances shown here, there are positive precipitation anomalies in the few days after surface impact, although the precipitation time series is noisier. The surface expressions span a few days either side of the surface impact date. This reflects the fact that the tracking algorithm is based on maximum values within a window with no backtracking and will therefore tend to reach the surface in the middle, or latter half of any surface expression.

The surface impacts of individual events are compared by centering on the date of surface impact (Figures 6–8) and composite means are calculated, shown as the top panel in each figure bounded in black. The anomalies are calculated over NW Europe, shown in the red box in Figure 9a. There is substantial variation between individual SSWs. On average, both split and displaced SSWs show a negative NAO around d_0 (Figure 6, top panel) and although the NAO is more negative (-0.51 compared with -0.40) for split events and persists for longer, these differences are not significant ($p > 0.1$).

Both types of event are on average associated with negative surface temperature anomalies over NW Europe around the surface impact date (Figure 7). However, unlike the NAO, mean surface temperature anomalies for split events are significantly more intense ($p < 0.05$) around the impact date. In addition, for the mean of split events, there are negative anomalies from 30 to around 7 days before surface impact, many of which are significantly lower than the displacement temperature anomalies ($p < 0.1$). Patterns are less systematically clear for precipitation anomalies (Figure 8). For displacement SSWs, there is a noticeable positive precipitation anomaly following surface impact, which is significantly different to the split SSW precipitation anomaly ($p < 0.05$). Although the magnitude of this may appear to be heavily influenced by the SSW event of March 4, 1981 more than two-thirds of displacement events show a positive precipitation anomaly immediately after the SSW onset and if the 1981 event is removed, the positive anomaly is still present. However, given the small sample size it is prudent to be cautious as the plots of individual events are quite noisy and differences could be attributable to sampling variability.

The difference in temperature and precipitation anomalies between displacements and split events, with little difference in the NAO, may be related to the latitude of the North Atlantic eddy-driven jet. Taking 5 days either side of the surface impact date, the jet is on average around 3° further south for split events compared with displacements. The more southerly jet may be associated with more extensive or intense cold-air outbreaks over Europe and increased blocking over the Northwest Atlantic, (e.g., Kolstad et al., 2010; Woollings et al., 2010). This variation in jet latitude will not necessarily project onto the NAO. The NAO only explains around 40% of large-scale atmospheric circulation variability over the North Atlantic region. Woollings et al. (2010) find that both the NAO and East Atlantic (EA) patterns describe combined changes in jet latitude and strength, and therefore it is important to consider both patterns when identifying jet stream changes. For example, an NAO index of -1 could represent a range of jet stream values, depending on the strength of the EA.

Patterns are qualitatively similar for the alternative classification (Figures S5–S7), with significant temperature anomaly differences ($p < 0.05$) around the time of surface impact. This indicates that the reshuffling of six events makes little difference, as they are of more marginal type. The positive precipitation anomaly for displacement events is still present (Figure S7) although is slightly weaker. When the ERA-I period only is considered mean features are still broadly similar (not shown).

Conceptually, the stratosphere can be thought of as a forcing boundary to the troposphere in some circumstances, and there will be an integration effect in the troposphere from such boundary forcings, including land surface temperature. However, we still find that the greatest differences from climatology are centered

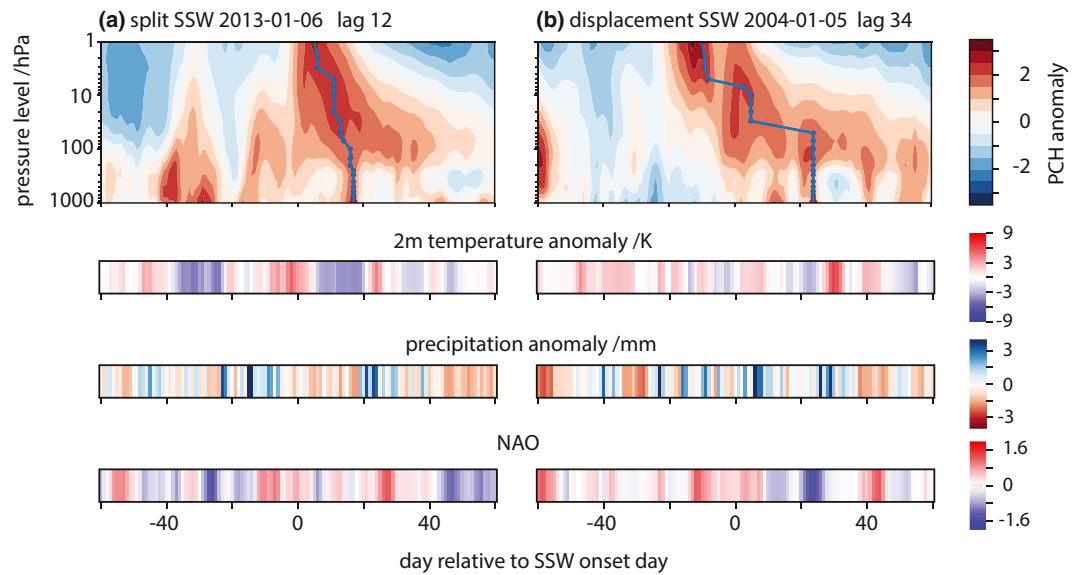


Figure 5. Downward tracking of SSW plotted on PCH anomalies, 2 mT and precipitation anomalies and the NAO Index, for 60 days before and after SSW onset for (a) a split SSW and (b) a displacement SSW.

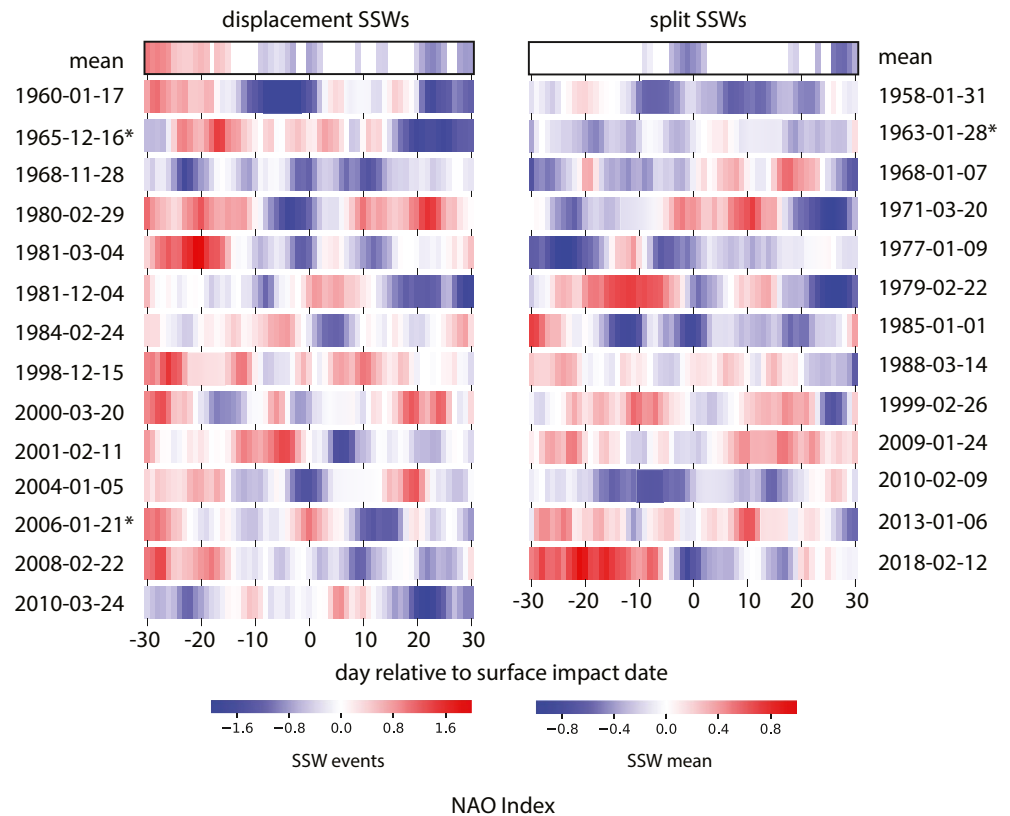


Figure 6. NAO values for 30 days before and after the SSW downtracking reaching the surface (d0). Note the bars are centered on the day the SSW reaches the surface, rather than SSW onset. The algorithm-sensitive events are marked with asterisk. Means of the events have a dark border and note the different scales. Means are masked so that daily mean values are only shown where at least two-thirds of the equivalent day in the individual events are of the same sign as the mean value. Dates are the SSW onset dates.

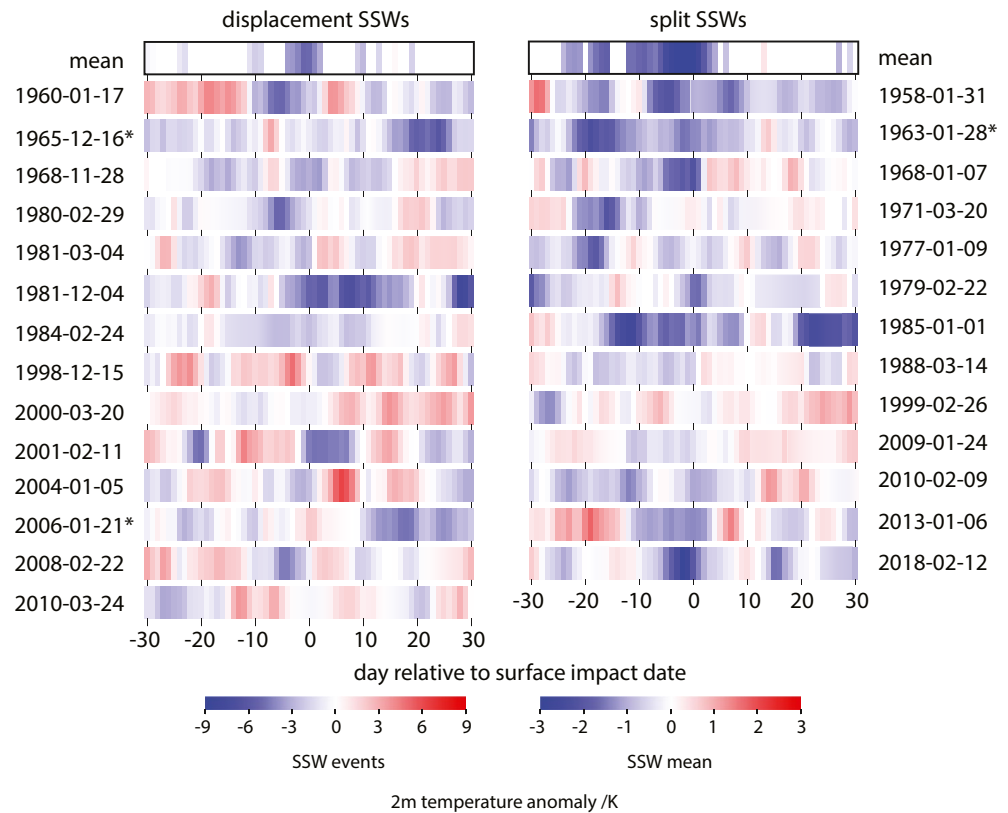


Figure 7. As Figure 6, but for surface temperature anomalies.

around the surface impact date. Shifts in the tropospheric jet latitude in response to changes in the SPV may occur instantaneously, while on other occasions the tropospheric response may be more influenced by internal variability, with a bias to weaker NAO and temperature anomalies from the boundary forcings.

4.5. Spatial Variability in Surface Temperature and Precipitation Anomalies

4.5.1. NW Europe

We next examine surface impacts over the wider European region, focusing on differences in impact between split and displacement events, using time-averaged values of temperature and precipitation anomalies over nonoverlapping 1-week intervals, for a 4-week period centered on d0 (Figure 9). Negative temperature anomalies over Europe accompany both displacement and split vortex events, but split events are accompanied by significantly lower temperature anomalies ($p < 0.05$) for the weeks immediately before and after d0 (Figures 9b and 9c). Cold anomaly differences are initially centered over the Low Countries for the second week prior to surface impact (Figure 9a). These then expand and intensify north eastwards to cover the UK and Scandinavia in the week before surface impact (Figure 9b). In the week after d0, the negative anomaly differences align west-east, with the greatest differences shifted eastward over Russia (Figure 9c). By two weeks after, the temperature anomaly differences between split and displacement events are weaker, and cold anomalies have shifted further east. King et al. (2019) found a similar impact on European temperatures for splits and displacements over a 30-day window. However, the true effect will be obscured by impacts and recoveries occurring at different times within the window. Centering anomalies on impact date overcomes this problem. For the UK in particular, split events are significantly colder than displacements averaged over the week before surface impact. Some of this may be associated with tropospheric precursors, while some will be linked to the SSW, as the surface impact date is not necessarily the first date at which a surface impact is evident, due to the tracking of maximum values within a window.

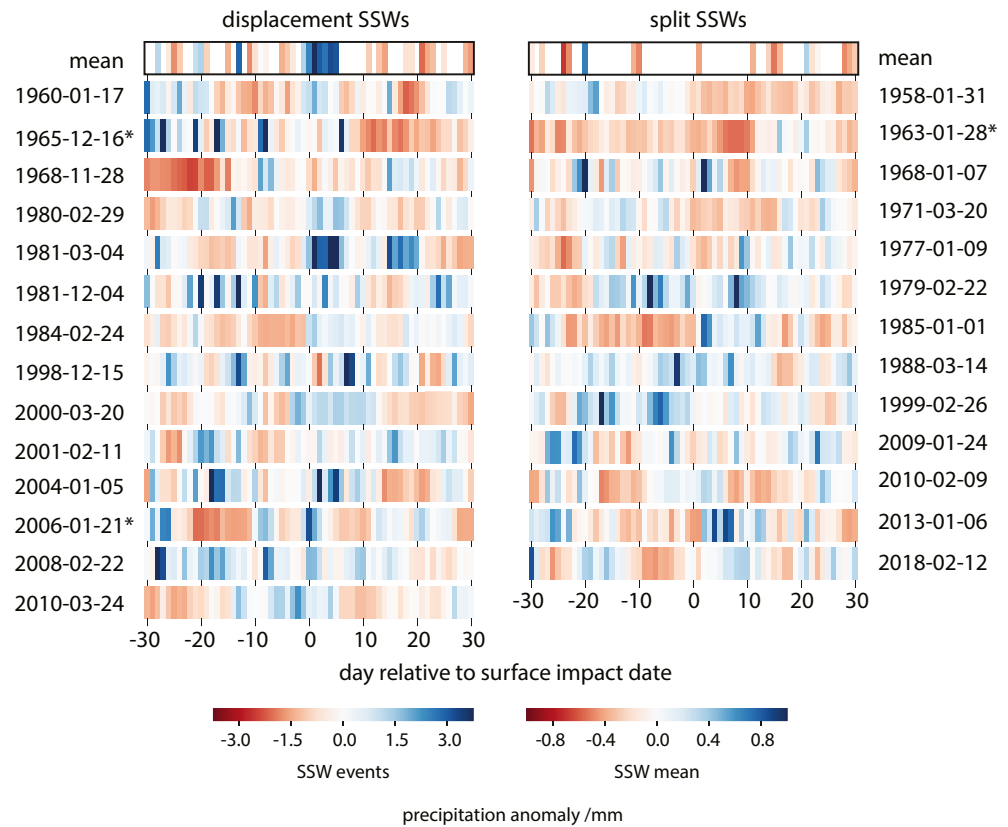


Figure 8. As Figure 6, but for precipitation anomalies.

Split events are wetter than displacements over much of Europe, but particularly over Italy and the Adriatic, over the week before surface impact (Figure 9f). However, in the week following surface impact, while southern Europe remains wetter for split events, NW Europe, focused on the British Isles, is noticeably drier (Figure 9g). For the weeks immediately prior to and after the date of surface impact, precipitation anomalies for both event types show a clear dipole, with positive anomalies to the south, over Europe and negative anomalies further north, over Greenland, Iceland, and Scandinavia indicative of a southward shift in the jet stream and a more negative NAO (not shown). This zonal shift in precipitation patterns is very evident in the week after surface impact in the western Atlantic. Both split and displaced events show a southward shift in the precipitation patterns and the associated jet and storm track, but for displaced events the pattern maintains a south-west-northeast tilt, while a much more zonal pattern is evident for splits, anomalies being confined to 30°N-45°N for the width of the Atlantic (Figure S8). Precipitation is increased over Spain for both split and displaced events (consistent with Ayarzagüena et al., 2018) but the increased precipitation in Mediterranean regions is greater for split events (in agreement with King et al., 2019), whereas for displaced events it is wetter over NW Europe. These results are consistent with the jet stream being displaced further south on average during the observed split events, although both events are associated with similar negative NAO values. The positive precipitation anomaly found in NW Europe for displacement events is a feature that may be obscured in the more usual averaging over longer windows related to SSW onset. Again, although the sample size is small, the tracking algorithm allows a more nuanced interpretation of data, compared with the averaging over long period of time and the combining of all SSW events.

4.5.2. The Northern Hemisphere

Figure 10 provides a wider context for the European surface temperature anomalies. The more negative temperature anomalies over Europe during split events in the weeks either side of d0 are the western extension of a region of negative temperature anomalies stretching across Eurasia to the Sea of Japan, which become more pronounced in the week after d0 (Figures 10f and 10g). A region of significant ($p < 0.05$)

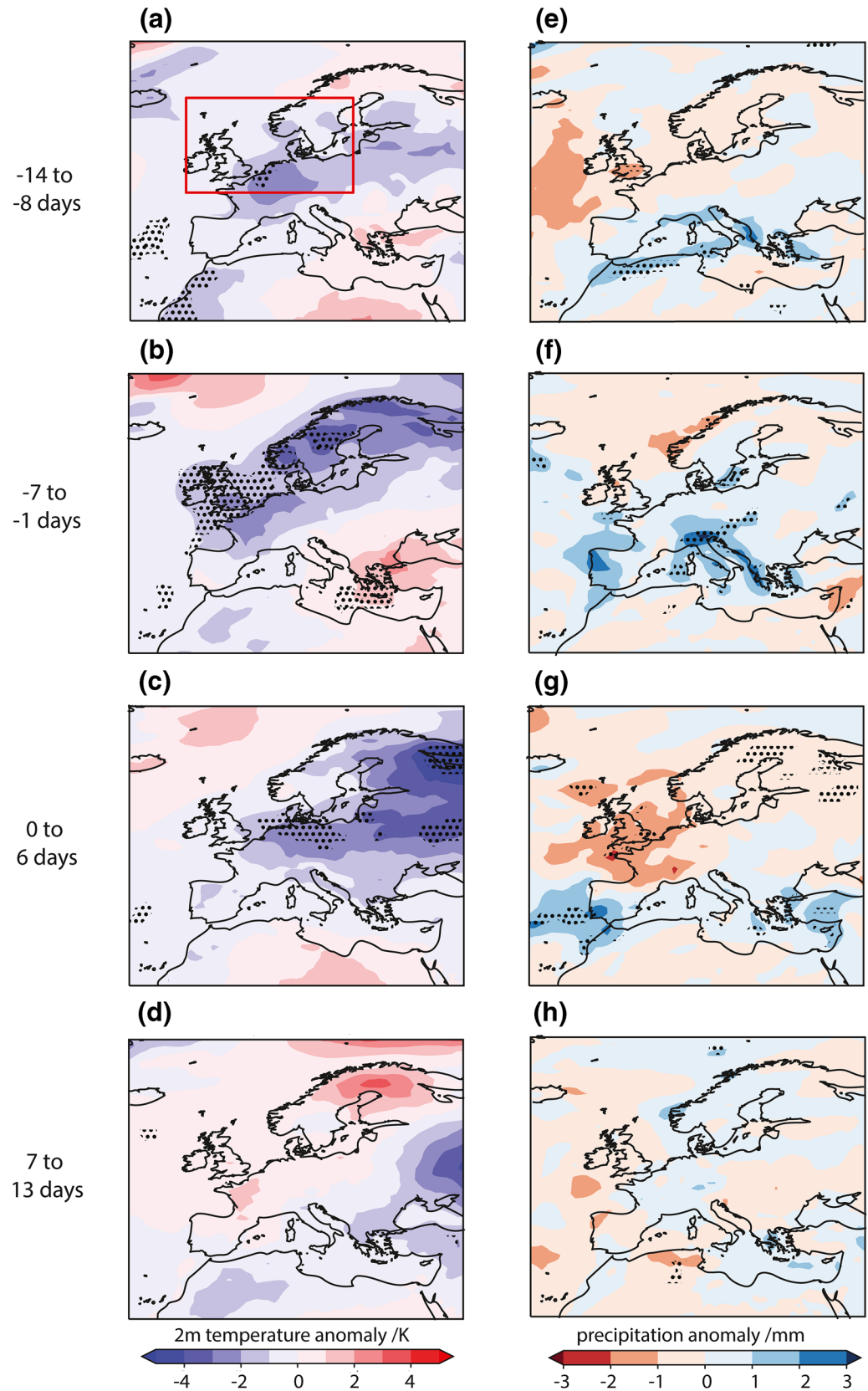


Figure 9. European surface temperature anomaly differences, (a–d) and precipitation anomaly differences (e–h), for split minus displacement events. Anomalies are averaged over 7-day periods for 2 weeks before and after the SSW surface impact date (here day 0). Significance stippled, $p < 0.05$ using permutation test, 10,000 resamples. Red box shows the reduced area used for the strips in Figures 5–8.

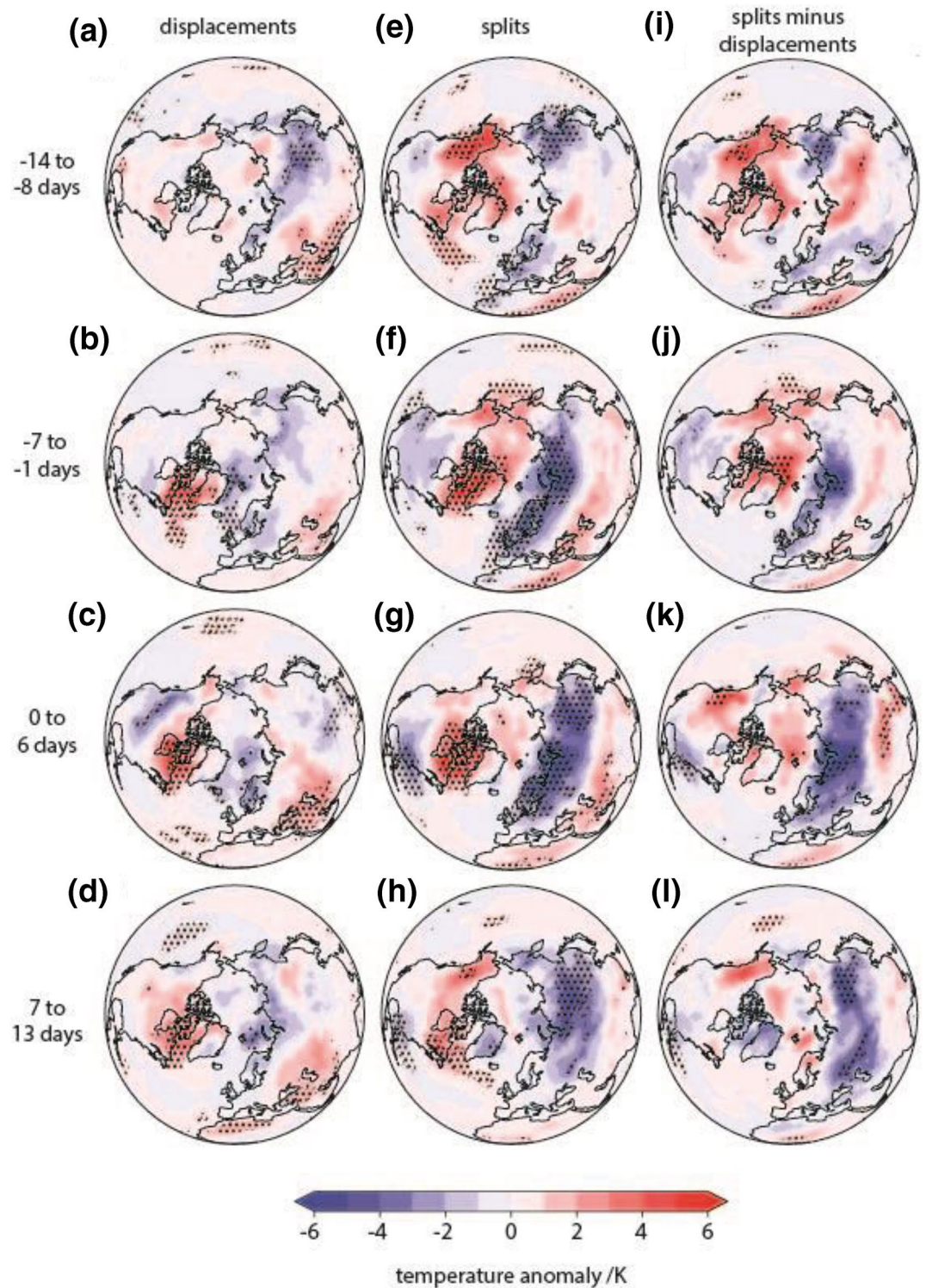


Figure 10. Surface temperature anomalies over the northern hemisphere for displacement, split, and split minus displacement events, for 7-day averaged periods before and after the surface impact date. Stippling shows area of significance ($p < 0.05$).

positive temperature anomalies is evident over the central Arctic two weeks prior to d0 for split events (Figure 10e). The difference between splits and displacements over the Arctic increases in the following week and both splits and displacements show warming over the Baffin Bay region in the weeks either side of d0, a feature of the negative NAO (Figures 10b, 10c, 10f, and 10g). In the week after surface impact, we see cooling to the west (east) of North America for displacement (split) events (Figures 10c and 10g) and the Eurasian cold anomalies intensify for the split events. By week 4, the split SSW Eurasian cold anomalies have contracted eastwards and become less intense (Figure 10h). For the modified classification, patterns are qualitatively similar although the Eurasian cold anomaly differences are less extensive and are located over Eastern Europe (not shown).

The hemispheric distribution of surface temperature anomalies for the week after surface impact, particularly for split events (Figure 10g), capture the main features of anomalies for all SSWs for 0–60 days after onset (see Butler et al., 2017, their Figure 4). We see notable positive anomalies over Baffin Bay and Hudson Bay and the Middle East and negative anomalies over the Eastern US and Eurasia. However, these anomalies are of a greater magnitude, resulting from a more targeted focus of the multievent mean on the date of surface impact. The differences between splits and displacement temperature anomalies at 0–6 days (Figure 10k) are similar to those seen by Mitchell et al. (2013) for the decay phase (0–60 days, their Figure 9i). In general, stronger surface impact from splitting events has been shown using reanalysis (Mitchell et al., 2013; Nakagawa & Yamazaki, 2006; W. J. M. Seviour et al., 2013) and free-running models (W. J. M. Seviour et al., 2016). Results here suggest that there are significant differences in the surface impact of split and displacement events, but these do not project strongly onto the NAO and AO/NAM, as discussed above. This may in part explain why studies examining impacts on the surface annular mode find little difference between splits and displacements (e.g., Maycock & Hitchcock, 2015), while when zonal asymmetries are considered, differences are more apparent (e.g., W. J. M. Seviour et al., 2016).

5. Summary

Our SSW tracking algorithm enables the objective tracing of polar cap anomalies from the stratosphere downwards through the troposphere. While we emphasize that the algorithm is empirical, and so cannot demonstrate causality, it does enable a novel separation of the timing and magnitudes of the surface impacts of individual events and multievent composites of displacement and split SSWs. The method is robust to variations in the tracking algorithm, can be applied to CMIP6 and other model data and results are similar for different definitions of split and displacement events, when a common set of onset dates is used.

The median downward tracking time for split events is found to be shorter than that of displacements, consistent with the more barotropic structure of such events (N. J. Matthewman & Esler, 2011; W. J. M. Seviour et al., 2016). We present for the first time the distribution of the timing of impact following the different types of SSW events (Figure 3c), and while the interquartile ranges completely overlap, the median displacement lag time is outside the interquartile range of the split lags.

Results here and elsewhere (Domeisen, 2019; Karpechko et al., 2017) suggest that not differentiating between nondownward-impacting and downward-impacting SSWs may obscure some of the impacts. When all SSW events are included, the median lags between split and displacement events are very similar. However, when the focus is on the subset of downward-impacting SSWs, the differences become more apparent and are unaffected by changes in event classification, given common onset dates.

While NAO impacts are similar, there are significant differences between how split and displacement SSWs impact on surface temperature. Split SSWs are associated with significantly more negative surface temperature anomalies over NW Europe, both before and at the time of surface impact. This is part of a pattern of lower temperature anomalies for split events which extends across Eurasia during the week either side of the surface impact date. Precipitation anomalies are always noisy, but split events are accompanied by wetter conditions over southern Europe and the Mediterranean, while NW Europe is wetter during displacement events. These patterns are consistent with the jet stream being further south following split events.

The algorithm will be useful for providing more targeted information about surface impacts of SSWs, both in terms of their timing and magnitude. It will be very useful for applying to model data and future projections,

to better identify any possible changes over time. In future work we will apply the algorithm to CMIP6 data and we will assess factors that may contribute to the different lag times found in this study.

Data Availability Statement

ERA-I and ERA40 data are freely available from the ECMWF website. ERA-I: <https://www.ecmwf.int/en/forecasts/datasets/reanalysis-datasets/era-interim>. ERA40: <https://apps.ecmwf.int/datasets/data/era40-daily/levtype%3Dsfc>. The NAO and AO indices are available from NOAA-CPC. NAO: <https://www.cpc.ncep.noaa.gov/products/precip/CWlink/pna/nao.shtml>. AO: https://www.cpc.ncep.noaa.gov/products/precip/CWlink/daily_ao_index/ao.shtml. Python code for the tracking algorithm is available from Zenodo (<https://doi.org/10.5281/zenodo.4279027>).

Acknowledgments

We acknowledge funding from the NERC “PEGASUS” project, grant number NE/S00985X/1. C. J. Wright acknowledges the Royal Society University Research Fellowship UF160545. We thank Andrew Charlton-Perez and one anonymous reviewer for valuable feedback that helped to improve the manuscript.

References

Ayarzaguena, B., Barriopedro, D., Garrido-Perez, J. M., Abalos, M., & de la Camara, A., (2018). Stratospheric Connection to the Abrupt End of the 2016/2017 Iberian Drought. *Geophysical Research Letters*, *45*(22), 12639–12646. <https://doi.org/10.1029/2018GL079802>

Baldwin, M. P., Ayarzaguena, B., Birner, T., Butchart, N., Butler, A. H., Charlton-Perez, A. J., et al. (2021). Sudden stratospheric warmings. *Reviews of Geophysics*, *59*(1), e2020RG000708. <https://doi.org/10.1029/2020RG000708>

Baldwin, M. P., & Dunkerton, T. J. (2001). Stratospheric harbingers of anomalous weather regimes. *Science*, *294*(5542), 581–584. <https://doi.org/10.1126/science.1063315>

Baldwin, M. P., & Thompson, D. W. J. (2009). A critical comparison of stratosphere-troposphere coupling indices. *Quarterly Journal of the Royal Meteorological Society*, *135*(644), 1661–1672. <https://doi.org/10.1002/qj.479>

Beerli, R., & Grams, C. M. (2019). Stratospheric modulation of the large-scale circulation in the Atlantic-European region and its implications for surface weather events. *Quarterly Journal of the Royal Meteorological Society*, *145*(725), 3732–3750. <https://doi.org/10.1002/qj.3653>

Butler, A. H., Sjöberg, J. P., Seidel, D. J., & Rosenlof, K. H. (2017). A sudden stratospheric warming compendium. *Earth System Science Data*, *9*(1), 63–76. <https://doi.org/10.5194/essd-9-63-2017>

Charlton, A. J., & Polvani, L. M. (2007). A new look at stratospheric sudden warmings. Part I: Climatology and modeling benchmarks. *Journal of Climate*, *20*(3), 449–469. <https://doi.org/10.1175/JCLI3996.1>

Charlton-Perez, A. J., Ferranti, L., & Lee, R. W. (2018). The influence of the stratospheric state on North Atlantic weather regimes. *Quarterly Journal of the Royal Meteorological Society*, *144*(713), 1140–1151. <https://doi.org/10.1002/qj.3280>

Charlton-Perez, A. J., & O'Neill, A. (2009). On the sensitivity of annular mode dynamics to stratospheric radiative timescales. *Journal of Climate*, *23*(2), 476–484. <https://doi.org/10.1175/2009JCLI2995.1>

Clark, J. P., & Feldstein, S. B. (2020). What drives the North Atlantic Oscillation's temperature anomaly pattern? Part I: The growth and decay of the surface air temperature anomalies. *Journal of the Atmospheric Sciences*, *77*(1), 185–198. <https://doi.org/10.1175/JAS-D-19-0027.1>

Cohen, J., & Jones, J. (2011). Tropospheric precursors and stratospheric warmings. *Journal of Climate*, *24*(24), 6562–6572. <https://doi.org/10.1175/2011JCLI4160.1>

Cropper, T., Hanna, E., Valente, M. A., & Jónsson, T. (2015). A daily Azores-Iceland North Atlantic Oscillation index back to 1850. *Geoscience Data Journal*, *2*(1), 12–24. <https://doi.org/10.1002/gdj3.23>

Dee, D. P., Uppala, S. M., Simmons, A. J., Berrisford, P., Poli, P., Kobayashi, S., et al. (2011). The ERA-Interim reanalysis: Configuration and performance of the data assimilation system. *Quarterly Journal of the Royal Meteorological Society*, *137*(656), 553–597. <https://doi.org/10.1002/qj.828>

Domeisen, D. I. V. (2019). Estimating the frequency of sudden stratospheric warming events from surface observations of the North Atlantic Oscillation. *Journal of Geophysical Research: Atmospheres*, *124*(6), 3180–3194. <https://doi.org/10.1029/2018JD030077>

Domeisen, D. I. V., Butler, A. H., Charlton-Perez, A. J., Ayarzaguena, B., Baldwin, M. P., Dunn-Sigouin, E., et al. (2020a). The role of the stratosphere in subseasonal prediction: 2. Predictability arising from stratosphere-troposphere coupling. *Journal of Geophysical Research: Atmospheres*, *125*(2), e2019JD030923. <https://doi.org/10.1029/2019JD030923>

Domeisen, D. I. V., Grams, C. M., & Papritz, L. (2020b). The role of North Atlantic-European weather regimes in the surface impact of sudden stratospheric warming events. *Weather and Climate Dynamics*, *1*(2), 373–388. <https://doi.org/10.5194/wcd-1-373-2020>

Duchon, C. E. (1979). Lanczos filtering in one and two dimensions. *Journal of Applied Meteorology*, *18*(8), 1016–1022.

Gerber, E. P., Martineau, P., Ayarzaguena, B., Barriopedro, D., Bracegirdle, T. J., Butler, A. H., et al. (2021). Extratropical stratosphere-troposphere coupling. In M. Fujiwara, G. L. Manney, L. Gray, & J. S. Wright (Eds.), *Stratosphere-troposphere processes and their role in climate (SPARC) reanalysis intercomparison project (S-RIP)*. Oberpfaffenhofen, Germany: SPARC (in press). www.sparc-climate.org/publications/sparc-reports

Hitchcock, P., & Simpson, I. R. (2014). The downward influence of stratospheric sudden warmings. *Journal of the Atmospheric Sciences*, *71*(10), 3856–3876. <https://doi.org/10.1175/JAS-D-14-0012.1>

Karpechko, A. Y., Charlton-Perez, A., Balmaseda, M., Tyrrell, N., & Vitart, F. (2018). Predicting sudden stratospheric warming 2018 and its climate impacts with a multimodel ensemble. *Geophysical Research Letters*, *45*(24), 13538–13546. <https://doi.org/10.1029/2018GL081091>

Karpechko, A. Y., Hitchcock, P., Peters, D. H. W., & Schneider, A. (2017). Predictability of downward propagation of major sudden stratospheric warmings. *Quarterly Journal of the Royal Meteorological Society*, *143*(704), 1459–1470. <https://doi.org/10.1002/qj.3017>

Kidston, J., Scaife, A. A., Hardiman, S. C., Mitchell, D. M., Butchart, N., Baldwin, M. P., & Gray, L. J. (2015). Stratospheric influence on tropospheric jet streams, storm tracks and surface weather. *Nature Geoscience*, *8*(6), 433–440. <https://doi.org/10.1038/ngeo2424>

King, A. D., Butler, A. H., Jucker, M., Earl, N. O., & Rudeva, I. (2019). Observed relationships between sudden stratospheric warmings and European climate extremes. *Journal of Geophysical Research: Atmospheres*, *124*(24), 13943–13961. <https://doi.org/10.1029/2019JD030480>

Kolstad, E. W., Breiteig, T., & Scaife, A. A. (2010). The association between stratospheric weak polar vortex events and cold air outbreaks in the Northern Hemisphere. *Quarterly Journal of the Royal Meteorological Society*, *136*(649), 886–893. <https://doi.org/10.1002/qj.620>

Lee, S. H., & Butler, A. H. (2020). The 2018–2019 Arctic stratospheric polar vortex. *Weather*, *75*(2), 52–57. <https://doi.org/10.1002/wea.3643>

- Lehtonen, I., & Karpechko, A. Y. (2016). Observed and modeled tropospheric cold anomalies associated with sudden stratospheric warmings. *Journal of Geophysical Research: Atmospheres*, *121*(4), 1591–1610. <https://doi.org/10.1002/2015JD023860>
- Martius, O., Polvani, L. M., & Davies, H. C. (2009). Blocking precursors to stratospheric sudden warming events. *Geophysical Research Letters*, *36*(14), L14806. <https://doi.org/10.1029/2009GL038776>
- Matsuno, T. (1971). A dynamical model of the stratospheric sudden warming. *Journal of the Atmospheric Sciences*, *28*(8), 1479–1494.
- Matthewman, N. J., & Esler, J. G. (2011). Stratospheric sudden warmings as self-tuning resonances. Part I: Vortex splitting events. *Journal of the Atmospheric Sciences*, *68*(11), 2481–2504. <https://doi.org/10.1175/JAS-D-11-07.1>
- Matthewman, N. J., Esler, J. G., Charlton-Perez, A. J., & Polvani, L. M. (2009). A new look at stratospheric sudden warmings. Part III: Polar vortex evolution and vertical structure. *Journal of Climate*, *22*(6), 1566–1585. <https://doi.org/10.1175/2008JCLI2365.1>
- Maycock, A. C., & Hitchcock, P. (2015). Do split and displacement sudden stratospheric warmings have different annular mode signatures? *Geophysical Research Letters*, *42*(24), 10943–10951. <https://doi.org/10.1002/2015GL066754>
- Mitchell, D. M., Charlton-Perez, A. J., & Gray, L. J. (2011). Characterizing the variability and extremes of the stratospheric polar vortices using 2D moment analysis. *Journal of the Atmospheric Sciences*, *68*(6), 1194–1213. <https://doi.org/10.1175/2010JAS3555.1>
- Mitchell, D. M., Gray, L. J., Anstey, J., Baldwin, M. P., & Charlton-Perez, A. J. (2013). The influence of stratospheric vortex displacements and splits on surface climate. *Journal of Climate*, *26*(8), 2668–2682. <https://doi.org/10.1175/JCLI-D-12-00030.1>
- Nakagawa, K. I., & Yamazaki, K. (2006). What kind of stratospheric sudden warming propagates to the troposphere? *Geophysical Research Letters*, *33*(4), L04801. <https://doi.org/10.1029/2005GL024784>
- Overland, J., Hall, R., Hanna, E., Karpechko, A., Vihma, T., Wang, M., & Zhang, X. (2020). The Polar Vortex and Extreme Weather: The Beast from the East in Winter 2018. *Atmosphere*, *11*(6), 664. <https://doi.org/10.3390/atmos11060664>
- Polvani, L. M., & Waugh, D. W. (2004). Upward wave activity flux as a precursor to extreme stratospheric events and subsequent anomalous surface weather regimes. *Journal of Climate*, *17*(18), 3548–3554. [https://doi.org/10.1175/1520-0442\(2004\)017<3548:UWAFAA>2.0.CO;2](https://doi.org/10.1175/1520-0442(2004)017<3548:UWAFAA>2.0.CO;2)
- Scherhag, R. (1952). Die explosionsartigen Stratosphärenwärmungen des Spätwinters 1951/52. *Berichte des Deutschen Wetterdienstes in der US-Zone*, *6*(1952), 51–63.
- Seviour, W. J. M., Gray, L. J., & Mitchell, D. M. (2016). Stratospheric polar vortex splits and displacements in the high-top CMIP5 climate models. *Journal of Geophysical Research: Atmospheres*, *121*(4), 1400–1413. <https://doi.org/10.1002/2015JD024178>
- Seviour, W. J. M., Mitchell, D. M., & Gray, L. J. (2013). A practical method to identify displaced and split stratospheric polar vortex events. *Geophysical Research Letters*, *40*(19), 5268–5273. <https://doi.org/10.1002/grl.50927>
- Tomassini, L., Gerber, E. P., Baldwin, M. P., Bunzel, F., & Giorgetta, M. (2012). The role of stratosphere-troposphere coupling in the occurrence of extreme winter cold spells over northern Europe. *Journal of Advances in Modeling Earth Systems*, *4*(4), M00A03. <https://doi.org/10.1029/2012MS000177>
- Uppala, S. M., Kallberg, P. W., Simmons, A. J., Andrae, U., Da Costa Bechtold, V., Fiorino, M., et al. (2005). The ERA-40 re-analysis. *Quarterly Journal of the Royal Meteorological Society*, *131*(612), 2961–3012. <https://doi.org/10.1256/qj.04.176>
- Waugh, D. W. (1997). Elliptical diagnostics of stratospheric polar vortices. *Quarterly Journal of the Royal Meteorological Society*, *123*(542), 1725–1748.
- Woollings, T., Hannachi, A., & Hoskins, B. (2010). Variability of the North Atlantic eddy-driven jet. *Quarterly Journal of the Royal Meteorological Society*, *136*(649), 856–868. <https://doi.org/10.1002/qj.625>